Proceedings of The Canadian Society for Mechanical Engineering International Congress 2014
CSME International Congress 2014
June 1-4, 2014, Toronto, Ontario, Canada

Ultrahigh Strength and Plastic Flow in Metal Nanotubes

Mingfei Sun and Fei Xiao
Department of Materials Science, Fudan University, Shanghai, China

Chuang Deng
Department of Mechanical Engineering, University of Manitoba, Winnipeg, MB Canada
dengc@ad.umanitoba.ca

Abstract— Metal nanowires are widely known for being strong but brittle due to the lack of plasticity and strain hardening in them. Here we report a new category of metal nanowires with hollow interior, metal nanotubes, to exhibit a combination of ultrahigh strength and extraordinary plastic flow during uniaxial tensile deformation through atomistic simulations. It is revealed that the metal nanotubes can maintain a ultrahigh plastic flow stress of more than 2 GPa up to ~ 60% tensile strain while the corresponding solid nanowires normally experience sharp yielding at less than 5% tensile strain at which the stress drops immediately to less than 1 GPa. Meanwhile, it is found that the yield strength and ductility in metal nanotubes can be up to ~ 40% and ~72% higher than the corresponding solid nanowires respectively by tuning the wall thickness.

Keywords: atomistic simulatoins; nanowire; nanotube; plasticity.

I. INTRODUCTION

Metal nanowires (NWs) have been widely observed to exhibit superior properties over their bulk counterparts mainly due to the high surface-to-volume ratio, especially the excellent mechanical properties including ultrahigh strength and large elastic limit[1–15]. On the other hand, carbon nanotubes (CNTs) have been long believed to be the strongest and stiffest materials yet discovered in terms of tensile strength and elastic modulus[16,17]. Stimulated by the extraordinary properties of both metal NWs and CNTs, metal nanotubes (NTs) have attracted growing interest in recent years. Approaches based on templating and electrodeposition[18–21]have been developed to grow large scale NTs in various metals, e.g., Au[22–25], Ag[26–29], Cu[30], etc. Depending on the synthesis method, both single crystalline [18,24,29,31,32] and polycrystalline [18,22] metal NTs have been produced with the outer diameter varying from less than 1 nm[27] to more than 100 nm[18] and wall thickness varying from a few atom layers[25,27] to tens of nanometers[18,24].

Nevertheless, despite the vast effort from both experiments and atomistic simulations that has been devoted to the research on metal NWs and CNTs, to date, only a few investigations via molecular dynamics (MD) have been performed on the mechanical characterization of metal NTs. Zheng et al. [33] have shown that in metal NTs while the outer surface was in tension as similar to that in metal NWs, either tension or compression could be achieved at the inner surface depending on the wall thickness. It is thus expected that the free surfaces may play a more complicated role in determining the mechanical properties of metal NTs than NWs. Ji and Park[34] have investigated the elasticity of squared Cu NTs oriented along [1 0 0] and [1 1 0] under tensile deformation by MD. They found that the yield strength, yield strain, and Young's modulus of Cu NTs all strongly depended on the NT orientation, the total surface area, and the amount of bulk materials that have been removed as compared to a solid NW. However, the atomistic details of the yielding process were not described and it is not clear how the metal NTs would deform when the wall thickness was reduced to a few atom layers[25,27]; the metal NTs may lose the crystallinity under such circumstances as found from experimental observations[25,27] and first principle computations[28]. Furthermore, it has been widely reported from both experiments and MD simulations that metal NWs lacked the ability to maintain plastic flow and experienced sharp yielding under uniaxial loading[1–3,7,11,35], which poses great challenge to the potential application of metal NWs as building blocks in future nanotechnology. To the best of our knowledge, no investigations have been done to characterize the plasticity of metal NTs.

In this study, MD simulations were performed to systematically investigate the plasticity of [1 1 0]-oriented single crystalline Au and Ag NTs under tensile deformation and compared with the corresponding Au and Ag NWs.

II. METHODS

MD simulations were performed using LAMMPS[36] to systematically investigate the elasticity and plasticity of single crystalline Au and Ag NTs with various diameters and wall thicknesses under tensile deformation. The interatomic forces were characterized by embedded-atom-method potentials for Au[37] and Ag[38] respectively. Cylindrical NTs oriented along [1 1 0] direction were created with fixed length of 50 nm. As shown in Figure 1, the radius of outer surface, radius of

This work was supported by Fudan University and the University of Manitoba, Canada.

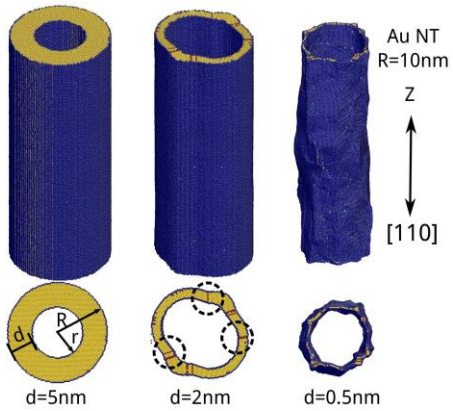

Figure 1. Side and top view of the atomistic configurations of relaxed Au NTs oriented along [1 1 0] direction with outer radius R = 10 nm and wall thickness d = 5 nm, 2 nm, and 0.5 nm. The dashed circles highlight the dislocations and stacking faults formed during the relaxation. The atom colors correspond to the local lattice orientation.

inner surface, and the wall thickness of a NT were defined as R, r, and d, respectively. A periodic boundary condition was imposed along the NT axis (z direction), while the NT was kept free in the other directions. The simulation timestep was 5 fs. Tensile deformation was performed at a constant strain rate of 10^8 s^{-1} along the axis using constant NVT integration for most of the simulations. A tensile strain rate of 10^9 s^{-1} was also used to expedite the deformation process in some of the simulations so that the fracture of NTs can be investigated. All the simulations were performed at 300 K. The tensile stress was calculated by adding the local Virial atomic stress[39] along the loading direction over all atoms and dividing by the deformed NT volume. In this study, the volume was calculated by multiplying the atomic volume by the total number of atoms. Since in most NTs (e.g., when d > = 1 nm) the crystalline structure was not significantly affected, a constant atomic volume has been assumed. AtomEye[40] was used to visualize the atomistic configurations. It is important to note that although both Au and Ag NTs have been simulated, only those based on Au were presented when the results were similar between Au and Ag NTs.

III. RESULTS

A. *Morphology of relaxed metal NTs*

Each model was relaxed for 100 *ps* under zero stress prior to any deformation. It was found that the morphologies of metal NTs would be significantly affected by the strong surface stress when the ratio of the wall thickness to the outer radius, *d/R*, was small. Some representative atomistic configurations were shown in Figure 1 for relaxed Au NTs with fixed outer radius (R = 10 nm) but varying wall thickness d. It was found that with decreasing d/R (decreasing d but constant R in Figure 1), the relaxed NT (e.g., when d = 1 nm and 2 nm) started to form structural defects such as dislocations and stacking faults (as highlighted by the dashed circles in Figure 1) although the original crystal structure and axial orientations were maintained. When d/R was further reduced, the plastic deformation induced by the surface stress was so strong that severe change of the surface morphology would be caused, e.g., Au NTs with wall thickness d = 0.5 nm in Figure 1. The wall thickness induced structural transition was similar to that was observed in FCC thin films[41]. The change in structure and morphology caused by the surface stress would significantly influence the elasticity and plasticity of metal NTs, as shown below.

B. *Ultrahigh yield strength in metal NTs*

Figure 2(a) showed the tensile stress-strain curves of Au NTs of fixed outer radius R = 10 nm but varying wall thickness from d = 0.5 nm to 2 nm. The corresponding solid NW was also simulated for reference. Some interesting points were recognized by analyzing the stress-strain curves of the Au NTs.

First of all, it can be seen from Figure 2(a) that the yield stress in Au NTs of R = 10 nm and d = 1 nm and above was significantly higher than that in the corresponding NW. In particular, the yield stress (σ_y = 3.79 GPa) in Au NT of R = 10 nm and d = 2 nm is ~ 42% higher than that in the corresponding NW ((σ_y = 2.66 GPa). The second important phenomenon noticed from Figure 2(a) was a dramatic transition from sharp yielding (e.g., the stress dropped sharply beyond the yield point) with high yield stress and no strain hardening to a relatively smooth yielding with low yield stress and pronounced strain hardening when the NT wall thickness was reduced to 1 nm and below. Such transition was

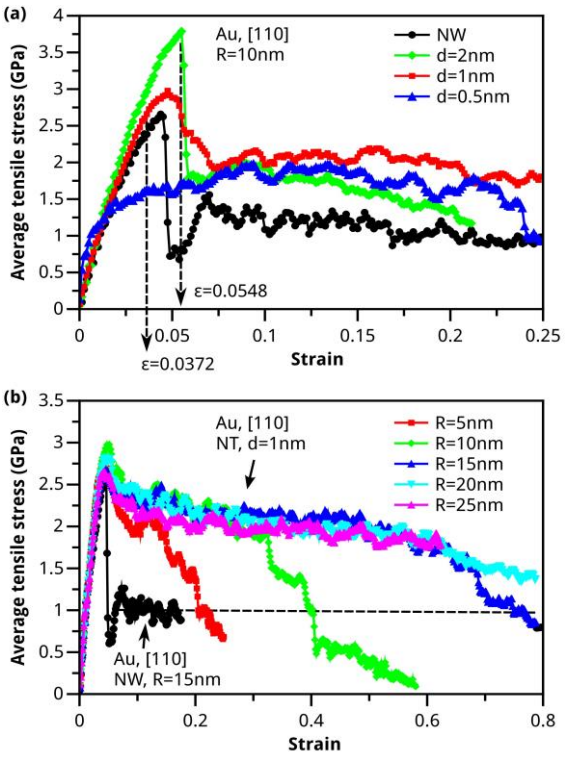

Figure 2. Tensile stress-strain curves in [1 1 0] Au NTs (a) of fixed outer radius R = 10 nm and varying wall thickness d = 0.5 nm, 1 nm, and 2 nm and (b) of fixed wall thickness d = 1 nm and outer radius varying from R = 5 nm to 25 nm. The vertical dashed lines in (a) indicate the strain at which the first dislocation nucleated in Au NT with d = 1 nm and 2 nm, respectively. The dashed line in (b) is added as a guide to the eye to indicate the plastic flow stress in [1 1 0] Au NW with R = 15 nm.

consistent with the atomistic configurations shown in Figure 1 that when the NT wall thickness was significantly reduced the NT would gradually lose the crystallinity. When the NT wall thickness d was 2 nm and above, the Au NTs (including NW) were crystalline and the yielding in them was dominated by surface dislocation nucleation as similar to that in metal NWs that have been reported before[42,43]. On the other hand, when d was reduced to 1 nm and below, the NTs can no longer be regarded as single crystalline (e.g., Figure 1 when d = 0.5 nm) where the dislocation nucleation was relatively easy and the plasticity was dominated by interactions between dislocations and the pre-formed structural defects during the initial relaxation.

C. Ultrahigh plastic flow in metal NTs

Whereas the ultrahigh strength in [1 1 0] Au NTs shown in Figure 2(a) was extraordinary, the plasticity in [1 1 0] Au NTs, on the other hand, was stimulating based on the stress-strain curves in Figure 2(a). For example, the plastic flow stress beyond the yield point in Au NT with d = 1 nm and R = 10 nm stayed consistently larger (> 2.0 GPa) than that in the corresponding NW (~ 1 GPa) at least before the tensile strain reached ε = 0.25. In order to further investigate the plasticity in

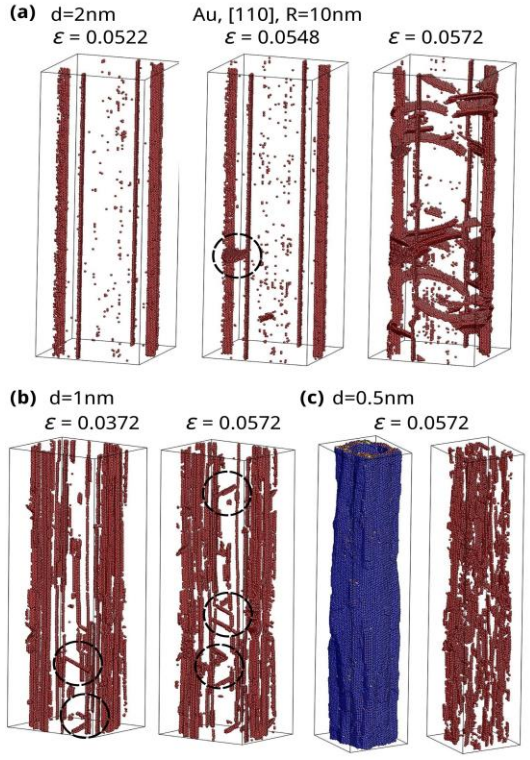

Figure 3. The atomistic configurations of [1 1 0] Au NTs with outer radius R = 10 nm and (a) wall thickness d = 2 nm immediately before the yield point (ε = 0.0522), at the yield point (ε = 0.0548), and immediately after the yield point (ε = 0.0572); (b) wall thickness d = 1 nm where the first dislocation nucleated (ε = 0.0372) and during typical plastic deformation (ε = 0.0572); (c) wall thickness d = 0.5 nm during typical plastic deformation (ε = 0.0572). The atom colors correspond to local lattice orientation and the perfect FCC atoms and free surface have been removed for clarity. All atoms are kept in the left atomic configuration in (c) to show the morphology of the free surface. Dashed circles are added in (b) to highlight the dislocation activities.

Au NTs, Au NTs with fixed wall thickness d = 1 nm and varying outer radius from R = 5 nm to 25 nm were simulated and compared to a solid NW of R = 15 nm. The stress-strain curves were plotted in Figure 2(b) which showed dramatically improved plasticity in [1 1 0] Au NTs when the outer radius was increased, e.g., when R = 15 nm and above. A dashed line was added in Figure 2(b) as a guide to the eye to indicate the plastic flow in the solid Au NW of R = 15 nm. In comparison with the solid NW, exceptionally high flow stress (> 2GPa) was maintained in Au NTs with R = 15 nm and above up to an ultra large tensile strain of ε = 0.6.

To find out the cause of ultrahigh plastic flow in [1 1 0] Au NTs, the atomistic configurations during the yielding process and plastic deformation were analyzed; representative results based on R = 10 nm were shown in Figure 3 where the atoms at free surfaces and perfect FCC lattice sites have been removed for clarity. It is found in Figure 3(a) that in [1 1 0] Au NT of d =2nm and R=10nm, a Shockley partial dislocation (highlighted by the dashed circle) was nucleated at the strain of ε = 0.0548, which corresponded to the yield point as indicated by the dashed arrow on the stress-strain curve in Figure 2(a). Immediately prior to the yielding (ε = 0.0522), no dislocations were nucleated besides the stacking faults formed during the relaxation process. It indicated that the pre-formed structural defects were stable during the deformation process. Immediately following the yield point (ε = 0.0572), dislocation propagation and escape from the free surfaces were found to dominate the plasticity, which led to sharp yielding and strain softening. In Au NT with d = 1 nm and R = 10 nm where ultrahigh plastic flow was observed, however, no clear yield point could be identified from the stress-strain curve (Figure 2(a)). It was found that dislocations were nucleated before reaching the maximum stress (Figure 3(b)), e.g., at ε = 0.0372 as indicated by the vertical dashed arrow in Figure 2(a). The nucleated dislocations could not move easily due to the confinement of the limited wall thickness and the large density of pre-existing obstacles formed during the relaxation process (Figure 2(b) at ε = 0.0572), which resulted in the strain hardening and superplasticity found in Figure 2. As the wall thickness was reduced to d = 0.5 nm, the dislocation activities became undefinable as indicated by Figure 3(c), where the plasticity was dominated by the structural defects that formed during the relaxation process (Figure 1).

D. Ultra-large ductility in metal NTs

Inspired by the superplasticity in Au NTs, we performed simulations at a strain rate of 109 s-1 in both Au and Ag NTs with fixed outer radius R = 10 nm but varying wall thickness d, so that the ultimate ductility and fracture mode could be investigated and compared with the corresponding NWs. The stress-strain curves were plotted in Figure 4(a) and (b), respectively, for Au and Ag NTs. The normalized fracture strain, $\varepsilon_f/\varepsilon_{f*}$($\varepsilon_{f*}$ was the fracture strain in the corresponding NW), was plotted in Figure 4(c). It is interesting to note from Figure 4 that while the fracture strain in most of the NTs was dramatically lower than that in the corresponding NW, the ultimate ductility in both Ag and Au NTs with d = 5 nm (or d/R = 0.5) was higher than their corresponding NWs. Specifically, an exceptional increase of ~ 72% in ductility was observed in

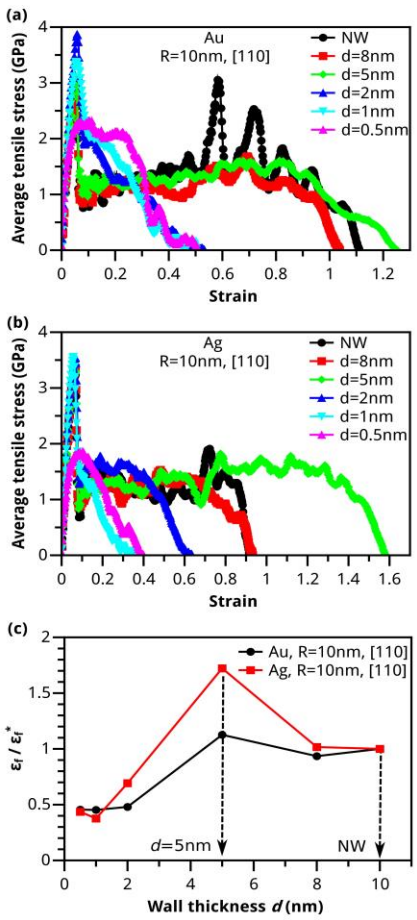

Figure 4. Tensile stress strain curves in [1 1 0] (a) Au and (b) Ag NTs (including the corresponding NWs) with outer radius R = 10 nm and varying wall thickness from d = 0.5 nm to 8 nm loaded at a strain rate of $10^9 s^{-1}$. (c) The normalized fracture strain in [1 1 0] Au and Ag NTs. Here ε_{f^*} represent the fracture strain of the corresponding NWs.

[1 1 0] Ag NT with d = 5 nm (or d/R = 0.5) as compared to the corresponding Ag NW. Future work will be needed to confirm if the ratio of d/R = 0.5 is the optimum value to enable best ductility in arbitrary metal NTs.

To find out why the ductility in metal NTs first increased and then decreased as the NT wall thickness was reduced (Figure 4(c)), the atomistic configurations of both Au and Ag NTs and the corresponding NWs at the fracture point were shown in Figure 5. For each NT (or NW), two atomistic configurations were presented. In the right configurations the atoms at the free surface and the perfect FCC lattice sites have been removed to show only the structural defects. It was found out that as the NT wall thickness changed, the fracture mode changed accordingly and the fracture modes were not the same between Au and Ag NTs of the same combination of R and d. As shown in Figure 5(a), dislocations were present only at locations close to the necking point in the solid Au NW, suggesting that during the plastic deformation dislocations could easily escape from the surface. In the Au NTs, on the contrary, residual dislocations were found to be able to stay in the NT. Furthermore, the residual dislocation density increased and distributed more uniformly as the wall thickness d was decreased. As the wall thickness was further decreased to d = 1 nm and 0.5 nm, however, the plasticity started to be controlled by the structural defects that formed during the initial structural relaxation, as shown in Figure 5(a). This trend agreed well with observations in Figure 4 that as the wall thickness decreased, the Au NTs experienced a transition from dislocation dominated plasticity to pre-formed defects dominated plasticity; such transition in plasticity mechanism may have resulted in the non-monotonic trend of ductility change in Figure 4(c). Additionally, while the general dislocation activities were found to be similar in Ag NTs (including the solid NW) with d = 5 nm and above, a new fracture mode was found in Ag NTs with d = 2 nm and below; the NT wall cracked before the ultimate fracture and failure of the whole NTs.

IV. Discussion and Summary

While exhibiting strong size effects on both the wall thickness and outer diameter, metal NTs also showed strong dependence on the axial orientation regarding both the strength and plasticity under uniaxial tension; the superplasticity shown in Figure 2(b) was not observed in Au and Ag NTs oriented along [1 0 0] and [1 1 1] directions. It is also worth mentioning that the superb mechanical properties in [1 1 0] metal NTs predicted in this study could be readily validated by experimental methods that have been widely used to test metal NWs. For example, the state-of-the-art in-situ tensile test facilities[3,44,45] could be directly applied to metal NTs. Although the applicable strain rate in experiments is usually several orders of magnitude lower than that in typical MD simulations, it could be inferred from the results obtained based on two different strain rates (e.g., Figure 2 and Figure 4) that at a much lower strain rate as similar to experimental conditions, the superplasticity in [1 1 0] Au NTs is likely to be maintained or even more pronounced than predicted in this study. A detailed analysis of the strain rate effects will be out of the scope of current study.

Furthermore, it is important to note that strain hardening has been rarely observed from past experiments on the tensile deformation of metal NWs. For example, Richter et al. [3] have performed in-situ tensile deformation of single crystalline Cu nanowiskers and found brittle failure with almost no plasticity. On the other hand, studies based on MD simulations[39] have suggested that high plastic flow and limited strain hardening (up to a few percent tensile strain) can be enabled in NWs through microstructural engineering, e.g., by introducing parallel nanoscale twin boundaries into Au NWs. Therefore, ultrahigh plastic flow and strain hardening up to a tensile strain of ~ 60% in metal NTs observed in this study was extraordinary and suggested an alternative approach of improving the plasticity in one-dimensional metal nanostructures. Above all, although a substantial amount of materials have been removed as compared to solid metal NWs, hollow metal NTs may be advantageous over corresponding metal NWs on almost every aspect in terms of mechanical properties, which deserve equivalent attention to, if not more than, that has been paid to metal NWs.

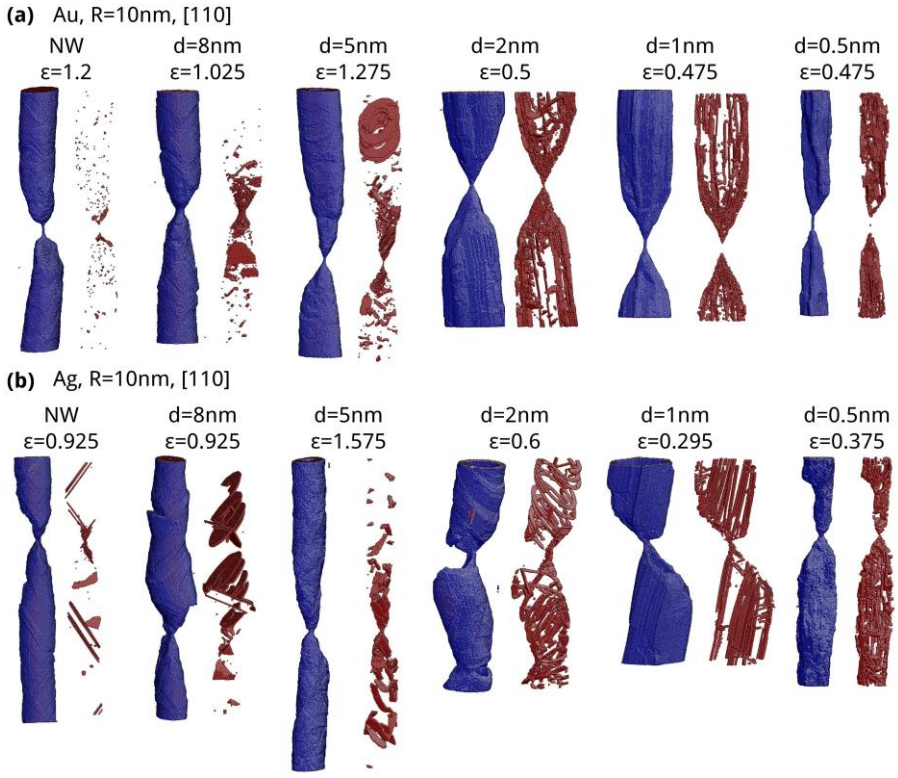

Figure 5. Atomistic configurations of [1 1 0] oriented (a) Au and (b) Ag NTs prior to the fracture point. The atom colors correspond to the local lattice orientation and the perfect FCC atoms and free surfaces have been removed in the configurations on the right to show the defects only.

In summary, we have used atomistic simulations to investigate the tensile properties of metal NTs. It was revealed that metal NTs may exhibit a combination of extraordinary strength, ultrahigh ductility and superplasticity as compared to their corresponding solid NWs by tuning the wall thickness, outer diameter, and the axial orientation. The structural defects pre-formed due to the strong surface stress when the wall thickness was extremely thin may have potentially contributed to the superplasticity in [1 1 0] metal NTs. Our study should stimulate experimental studies towards the synthesis and mechanical characterization of superlight, strong, and ductile metal NTs.

ACKNOWLEDGMENT

This work was enabled by the use of computing resources provided by WestGrid and Compute/Calcul Canada.

REFERENCES

[1] J.R. Greer, J.-Y. Kim, M.J. Burek, The in-situ mechanical testing of nanoscale single-crystalline nanopillars, JOM J. Miner. Met. Mater. Soc. 61 (2009) 19–25.

[2] J. Wang, F. Sansoz, J. Huang, Y. Liu, S. Sun, Z. Zhang, et al., Near-ideal theoretical strength in gold nanowires containing angstrom scale twins, Nat. Commun. 4 (2013) 1742.

[3] G. Richter, K. Hillerich, D.S. Gianola, R. Monig, O. Kraft, C.A. Volkert, Ultrahigh strength single crystalline nanowhiskers grown by physical vapor deposition, Nano Lett. 9 (2009) 3048–3052.

[4] B. Wu, A. Heidelberg, J.J. Boland, J.E. Sader, Sun, Li, Microstructure-Hardened Silver Nanowires, Nano Lett. 6 (2006) 468–472.

[5] B. Wu, A. Heidelberg, J.J. Boland, Mechanical properties of ultrahigh-strength gold nanowires, Nat. Mater. 4 (2005) 525–529.

[6] K. Gall, J. Diao, M.L. Dunn, The strength of gold nanowires, Nano Lett. 4 (2004) 2431–2436.

[7] A.T. Jennings, J.R. Greer, Tensile deformation of electroplated copper nanopillars, Philos. Mag. 91 (2011) 1108–1120.

[8] T. Zhu, J. Li, S. Ogata, S. Yip, Mechanics of ultra-strength materials, MRS Bull. 34 (2009) 167.

[9] W. Liang, M. Zhou, Response of copper nanowires in dynamic tensile deformation, Proc. Inst. Mech. Eng. Part C J. Mech. Eng. Sci. 218 (2004) 599–606.

[10] F. Tavazza, L.E. Levine, A.M. Chaka, Elongation and breaking mechanisms of gold nanowires under a wide range of tensile conditions, J. Appl. Phys. 106 (2009) 043522–043522.

[11] C. Deng, F. Sansoz, Near-Ideal strength in gold nanowires achieved through microstructural design, ACS Nano. 3 (2009) 3001–3008.

[12] M.B. Lowry, D. Kiener, M.M. LeBlanc, C. Chisholm, J.N. Florando, J.W. Morris Jr., et al., Achieving the ideal strength in annealed molybdenum nanopillars, Acta Mater. 58 (2010) 5160–5167.

[13] S. Hao, L. Cui, D. Jiang, X. Han, Y. Ren, J. Jiang, et al., A Transforming Metal Nanocomposite with Large Elastic Strain, Low Modulus, and High Strength, Science. 339 (2013) 1191–1194.

[14] Y. Yue, N. Chen, X. Li, S. Zhang, Z. Zhang, M. Chen, et al., Crystalline Liquid and Rubber-Like Behavior in Cu Nanowires, Nano Lett. 13 (2013) 3812–3816.

[15] Y. Yue, P. Liu, Z. Zhang, X. Han, E. Ma, Approaching the theoretical elastic strain limit in copper nanowires, Nano Lett. 11 (2011) 3151–3155.

[16] B. Peng, M. Locascio, P. Zapol, S. Li, S.L. Mielke, G.C. Schatz, et al., Measurements of near-ultimate strength for multiwalled carbon nanotubes and irradiation-induced crosslinking improvements, Nat. Nanotechnol. 3 (2008) 626–631.

[17] M.-F. Yu, O. Lourie, M.J. Dyer, K. Moloni, T.F. Kelly, R.S. Ruoff, Strength and breaking mechanism of multiwalled carbon nanotubes under tensile load, Science. 287 (2000) 637–640.

[18] Y. Sun, B. Mayers, Y. Xia, Metal nanostructures with hollow interiors, Adv. Mater. 15 (2003) 641–646.

[19] H. Cao, L. Wang, Y. Qiu, Q. Wu, G. Wang, L. Zhang, et al., Generation and growth mechanism of metal (Fe, Co, Ni) nanotube arrays, ChemPhysChem. 7 (2006) 1500–1504.
[20] M. Wirtz, M. Parker, Y. Kobayashi, C.R. Martin, Template-Synthesized Nanotubes for Chemical Separations and Analysis, Chem.- Eur. J. 8 (2002) 3572–3578.
[21] C. Mu, Y.-X. Yu, R.M. Wang, K. Wu, D.S. Xu, G.-L. Guo, Uniform metal nanotube arrays by multistep template replication and electrodeposition, Adv. Mater. 16 (2004) 1550–1553.
[22] H. Zhu, H. Chen, J. Wang, Q. Li, Fabrication of Au nanotube arrays and their plasmonic properties, Nanoscale. 5 (2013) 3742–3746.
[23] H.-W. Wang, C.-F. Shieh, H.-Y. Chen, W.-C. Shiu, B. Russo, G. Cao, Standing [111] gold nanotube to nanorod arrays via template growth, Nanotechnology. 17 (2006) 2689.
[24] Y. Sun, B.T. Mayers, Y. Xia, Template-engaged replacement reaction: a one-step approach to the large-scale synthesis of metal nanostructures with hollow interiors, Nano Lett. 2 (2002) 481–485.
[25] Y. Oshima, A. Onga, K. Takayanagi, Helical gold nanotube synthesized at 150 K, Phys. Rev. Lett. 91 (2003) 205503.
[26] M. Davenport, K. Healy, Z.S. Siwy, Ag nanotubes and Ag/AgCl electrodes in nanoporous membranes, Nanotechnology. 22 (2011) 155301.
[27] M.J. Lagos, F. Sato, J. Bettini, V. Rodrigues, D.S. Galvão, D. Ugarte, Observation of the smallest metal nanotube with a square cross-section, Nat. Nanotechnol. 4 (2009) 149–152.
[28] P.A.S. Autreto, M.J. Lagos, F. Sato, J. Bettini, A.R. Rocha, V. Rodrigues, et al., Intrinsic Stability of the Smallest Possible Silver Nanotube, Phys. Rev. Lett. 106 (2011) 065501.
[29] J. Sun, J. Zhang, W. Liu, S. Liu, H. Sun, K. Jiang, et al., Shape-controlled synthesis of silver nanostructures, Nanotechnology. 16 (2005) 2412.
[30] M. Venkata Kamalakar, A.K. Raychaudhuri, A novel method of synthesis of dense arrays of aligned single crystalline copper nanotubes using electrodeposition in the presence of a rotating electric field, Adv. Mater. 20 (2008) 149–154.
[31] P. Mohanty, T. Kang, B. Kim, J. Park, Synthesis of single crystalline tellurium nanotubes with triangular and hexagonal cross sections, J. Phys. Chem. B. 110 (2006) 791–795.
[32] J.Y. Guo, C.X. Xu, A.M. Hu, K.D. Oakes, F.Y. Sheng, Z.L. Shi, et al., Sintering dynamics and thermal stability of novel configurations of Ag clusters, J. Phys. Chem. Solids. (2012).
[33] J. Zhang, C. Wang, R. Chowdhury, S. Adhikari, Small-scale effect on the mechanical properties of metallic nanotubes, Appl. Phys. Lett. 101 (2012) 093109.
[34] C. Ji, H.S. Park, Characterizing the elasticity of hollow metal nanowires, Nanotechnology. 18 (2007) 115707.
[35] B. Hyde, H.D. Espinosa, D. Farkas, An atomistic investigation of elastic and plastic properties of Au nanowires, Jom. 57 (2005) 62–66.
[36] S. Plimpton, Fast Parallel Algorithms for Short-Range Molecular Dynamics, J. Comput. Phys. 117 (1995) 1–19.
[37] G. Grochola, S.P. Russo, I.K. Snook, On fitting a gold embedded atom method potential using the force matching method, J. Chem. Phys. 123 (2005) 204719.
[38] P.L. Williams, Y. Mishin, J.C. Hamilton, An embedded-atom potential for the Cu–Ag system, Model. Simul. Mater. Sci. Eng. 14 (2006) 817–833.
[39] C. Deng, F. Sansoz, Enabling Ultrahigh Plastic Flow and Work Hardening in Twinned Gold Nanowires, Nano Lett. 9 (2009) 1517–1522.
[40] J. Li, AtomEye: an efficient atomistic configuration viewer, Model. Simul. Mater. Sci. Eng. 11 (2003) 173.
[41] A. Hasmy, E. Medina, Thickness induced structural transition in suspended fcc metal nanofilms, Phys. Rev. Lett. 88 (2002) 096103.
[42] C. Deng, F. Sansoz, Size-dependent yield stress in twinned gold nanowires mediated by site-specific surface dislocation emission, Appl. Phys. Lett. 95 (2009) 091914–091914.
[43] C. Deng, F. Sansoz, Repulsive force of twin boundary on curved dislocations and its role on the yielding of twinned nanowires, Scr. Mater. 63 (2010) 50–53.
[44] D.S. Gianola, C. Eberl, Micro-and nanoscale tensile testing of materials, JOM. 61 (2009) 24–35.
[45] Y. Zhu, H.D. Espinosa, An electromechanical material testing system for in situ electron microscopy and applications, Proc. Natl. Acad. Sci. U. S. A. 102 (2005) 14503–14508.